Enhancing visible-light photocatalytic activity of α-Bi_2O_3 via non-metal N and S doping*

Shang Jun(尚 军), Gao Yuan(高 远), Hao Wei-Chang(郝维昌)†, Jing Xi(井 溪), Xin Hui-Ju(信会菊), Wang Liang(王 亮), Feng Hai-Feng(冯海凤), and Wang Tian-Min(王天民)

Center of Materials Physics and Chemistry and Department of Physics, Beihang University, Beijing 100191, *China*

(Received 24 June 2013; revised manuscript received 21 August 2013; published online 24 January 2014)

In recent years, some important research indicated that the visible-light activity of photocatalysts could be enhanced via incorporating p-block non-metal elements into the lattice. In this paper, we investigated the electronic structures of pure and different non-metal (C, N, S, F, Cl, and Br) doped α-Bi_2O_3 using first-principles calculations based on the density functional theory. The band structures, the electronic densities of states, and the effective masses of electrons and holes for doped α-Bi_2O_3 were obtained and analyzed. The N and S dopings narrowed the band gap and reduced the effective mass of the carriers, which are beneficial for the photocatalytic performance. The theoretical predication was further confirmed by the experimental results.

Keywords: α-Bi_2O_3, first-principles calculation, non-metal doping, photocatalytic performance

PACS: 81.07.Bc, 68.37.Og, 84.60.Jt **DOI:** 10.1088/1674-1056/23/3/038103

1. Introduction

Nowadays, semiconductor-based photocatalysts have received increasing attention due to their potential applications in environmental pollution purification[1–3] and energy conversion.[4–6] TiO_2 is considered as a typical photocatalyst and has been widely studied for its outstanding stability and high photocatalytic activity.[7–11] However, TiO_2 can only utilize the ultraviolet irradiation which occupies no more than 4% of the solar spectrum owing to its relatively wide band gap (3.2 eV).[9] To date, great efforts have been made to explore visible-light photocatalysts. It has proved to be very successful in the enhancement of visible-light activity via incorporating p-block non-metal elements into transition metal oxides such as $TiO_{2-x}M_x$ (M = N, C, B, S),[12–15] TaON,[16] $LaTiO_2N$,[17] and $Sm_2TiS_2O_5$.[18] The incorporated non-metal elements participate in the formation of the top of the valence band (VB), which results in the up-shift of the VB and narrowing of the band gap.[19] Moreover, the hybridization between non-metal np states and O 2p states can lead to a highly dispersive VB.[20] The dispersive band structure means that the effective mass of the hole is light, which is advantageous for the transfer of photo-induced charge carriers.[21]

As an important metal-oxide semiconductor, bismuth oxide (Bi_2O_3) has attracted growing interest for years.[22–25] There are mainly four polymorphs of bismuth oxide, noted as α-, β-, γ-, and δ-Bi_2O_3.[26] Among them, the monoclinic α-Bi_2O_3 remains stable at room temperature.[26] Bi_2O_3 is believed to be a potential visible-light-driven photocatalyst because of its remarkable photoconductivity and relatively narrow band gap (2.85 eV).[27,28] However, the photocatalytic activity of Bi_2O_3 in the visible-light region is not satisfactory, and we believe there is still room to further optimize the performance of Bi_2O_3. Inspired by the case of TiO_2, we expect that incorporating non-metal elements into Bi_2O_3 could be a promising route to further improve the visible-light photocatalytic activity of Bi_2O_3.

In this article, we study the electronic structures of pure and different p-block non-metal elements (C, N, S, F, Cl and Br) doped α-Bi_2O_3 systems by first-principles calculations. The geometry is optimized. The band structures, the electronic densities of states (DOS), and the effective mass of carriers are obtained. The visible-light photocatalytic activities of N and S doped α-Bi_2O_3 are improved compared with that of pure α-Bi_2O_3. The experimental results validate the theoretical simulation very well. Meanwhile, some suggestions are given on how to effectively adjust the electronic structures of α-Bi_2O_3 and other oxides by non-metal element doping for enhancing the visible-light photocatalytic performance.

2. Computation and experimental details

2.1. Computation method

α-Bi_2O_3 has a monoclinic structure and belongs to the $P121/C1$ space group with measured lattice parameters a = 5.8499 Å, b = 8.1698 Å, c = 7.5123 Å, β = 112.988°. Our calculations were performed with a 40-atom supercell, containing 16 Bi atoms and 24 O atoms in two unit cells stacking along the b axis. In this paper, we obtained doped α-Bi_2O_3 via replacing O with a non-metal element. The impurity concentration (atomic fraction) of the doped system $Bi_{16}O_{23}M$ (M =

*Project supported by the National Natural Science Foundation of China (Grant Nos. 51072012 and 51272015).

†Corresponding author. E-mail: whao@buaa.edu.cn

© 2014 Chinese Physical Society and IOP Publishing Ltd

C, S, N, F, Cl, Br) was 4.17%. The crystal structure is shown in Fig. 1.

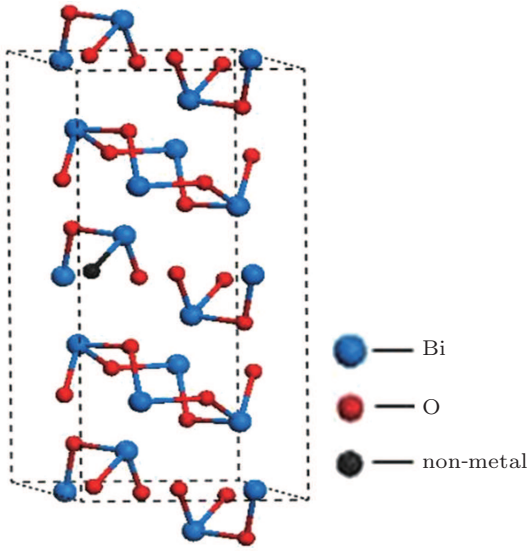


Fig. 1. (color online) Structure of the supercell for $Bi_{16}O_{23}M$ (M = S, N, C, F, Cl, Br).

All the first-principles calculations were carried out with the CASTEP codes of Material Studio (MS) based on the density functional theory (DFT), using the plane-wave ultrasoft pseudopotential for the interaction between the ion core and the valence electrons. The exchange and correlation functional was described by the Perdew–Burke–Ernzerhof (PBE) functional, one of the most famous and widely used generalized gradient approximations (GGA). The valence electrons discussed in this paper were $6s^26p^3$ for Bi, $2s^22p^4$ for O, $2s^22p^2$ for C, $2s^22p^3$ for N, $3s^23p^4$ for S, $2s^22p^5$ for F, $3s^23p^5$for Cl, and $4s^24p^5$ for Br. The energy cutoff for the plane wave basis was set at 380 eV, and a 5×4×4 grid of special k-points was used for the Brillouin zone integration. The relaxation process was considered converged when the self-consistent convergence of the total energy was better than 1.0×10^{-5} eV/atom. The force, the stress, and the displacement of each atom were no more than 0.03 eV/Å, 0.05 GPa, and 0.001 Å, respectively.

2.2. Experimental details

2.2.1. Preparation of catalyst

Pure and S doped α-Bi_2O_3 were synthetized by a simple chemical precipitation method. In a typical case, 1.94 g $Bi(NO_3)_3{\cdot}5H_2O$ was dissolved in 20 mL dilute nitric acid (1 mol/L) to prevent the hydrolyzation of Bi^{3+} ions. Then, certain amounts of cetrimonium bromide (CTAB) used as the surfactant and thiourea used as the source of S were added into the above solution under sustained stirring. 200 mL NaOH aqueous solution (0.21 mol/L) was slowly dropped into the solution after it became homogeneous. With constant stirring for 30 min, white precipitates formed in the above solution. Finally, the obtained solids were dried at 353 K for 8 h and then calcined at 773 K in air for 2 h. We prepared N doped α-Bi_2O_3 by the atmosphere calcination method. A certain amount of the above prepared α-Bi_2O_3 was calcined in a tube furnace at 573 K under NH_3 flow for 3 h. The exhaust was carefully treated with acid to avoid environmental pollution.

2.2.2. Photocatalytic activity evaluation

The visible-light photocatalytic activity of pure and N/S doped α-Bi_2O_3 was evaluated by the degradation of rhodamine B (RhB) in aqueous solution. The optical system for detecting the catalytic reaction included a 350 W Xenon lamp with a UV cut-off filter ($\lambda \geq 420$ nm). Before illumination, an 80 mL suspension of RhB (0.02 mmol/L) with 0.1 g Bi_2O_3 or N/S doped Bi_2O_3 was magnetically stirred in the dark for 60 min to reach the adsorption/desorption equilibrium. Then, the suspension was irradiated by the 350 W Xenon lamp and analyzed at regular intervals by a UV–Vis spectrophotometer.

X-ray photoelectron spectroscopy (XPS) was checked by a PHI Quantera SXM equipment in Tsinghua University. The energy of X-ray was 2 kV. The X-ray absorption near edge structure (XANES) was obtained at the X-ray absorption fine structure station of Beijing Synchrotron Radiation Facility of the Institute of High Energy Physics, Chinese Academy of Sciences.

3. Results and discussion

3.1. Electron structure computation

α-Bi_2O_3 is optimized by using the CASTEP codes in the MS program with the GGA. We obtain the equilibrium lattice parameters $a = 5.8968$ Å, $b = 8.1691$ Å, $c = 7.4461$ Å, $\beta = 112.232°$ which are in good agreement with the JCPDS file No. 41-1449 (space group $P121/C1$, $a = 5.8499$ Å, $b = 8.1698$ Å, $c = 7.5123$ Å, $\beta = 112.988°$). Because of the differences in ion radius and electronic states, a lattice distortion usually occurs when other ions incorporate into the host lattice. So we obtain the equilibrium lattice parameters of the doped system $Bi_{16}O_{23}M$ (M = C, N, S, F, Cl, Br) and compare them with those of pure Bi_2O_3 (shown in Table 1). The lattice distortions are not serious. Thus, the doped α-Bi_2O_3 can remain its parent structure.

Table 1. Calculated lattice distortion of non-metal doped system $Bi_{16}O_{23}M$ (M = C, N, S, F, Cl, Br) compared to pure α-Bi_2O_3.

	Δa/Å	Δb/Å	Δc/Å	$\Delta\beta$/(°)	ΔV/Å^3
C–O	–0.019	0.085	–0.124	–1.01	–5.31
N–O	–0.032	0.052	–0.061	–0.59	–4.11
S–O	0.021	0.103	0.034	–1.509	12.09
F–O	0.015	0.011	0.019	0.45	0.74
Cl–O	0.101	0.081	0.143	1.65	19.26
Br–O	0.135	0.169	0.181	1.99	28.38

Figure 2 shows the calculated band structure and DOS of pure α-Bi_2O_3. It has a direct band gap. The calculated band

gap is 2.39 eV, smaller than the reported value of 2.58 eV[27] due to the well-known GGA weakness. It is important to note that the top of the VB with a flat dispersion is composed of O 2p as well as some parts of the hybridized Bi 6s6p orbitals, while the bottom of the CB is composed of the hybridized Bi 6p and a small amount of Bi 6s and O 2p orbitals. These characteristics are in good accordance with the previous calculations.[26]

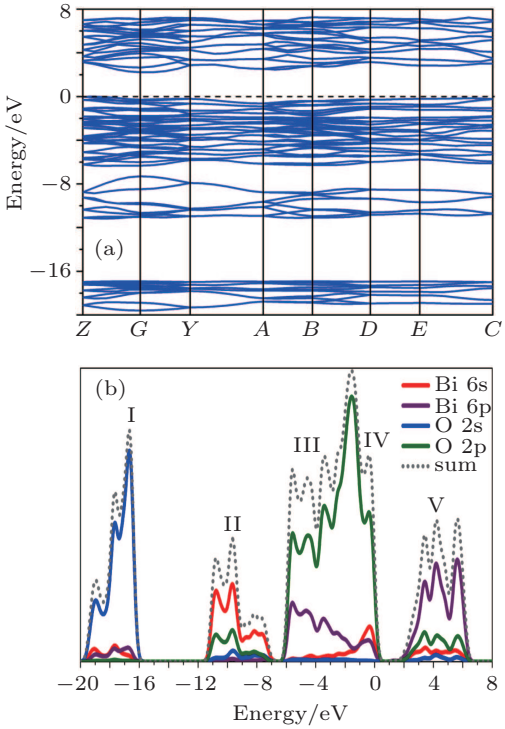


Fig. 2. (color online) (a) The band structure, (b) total and partial densities of states of pure α-Bi_2O_3.

We obtain the doped α-Bi_2O_3 via replacing O with non-metal elements, calculated their electron structures and compared them with that of pure α-Bi_2O_3. Figure 3 shows the band structures of non-metal doped system $Bi_{16}O_{23}M$ (M = C, N, S, F, Cl, Br). They all have a direct band gap, and the band gaps are narrower than that of α-Bi_2O_3. The incorporation of S narrows the band gap most obviously with a decrease of 0.71 eV, followed by N with a decrease of 0.61 eV. For both S and N dopings, the bottom of the CB shifts down apparently while the VB broadens and becomes more dispersive. As a result, the band gap is obviously narrowed, which is beneficial for the enhancement of the photocatalytic performance. The band gap of the halogen element (F, Cl, and Br) doped α-Bi_2O_3 decreases slightly with the increase of the atomic number, and both the VB and the CB shift down significantly compared to those of pure Bi_2O_3. Impurity bands appear near the Fermi level for C, F, Cl, and Br dopings, which may make the transfer of electrons easier.

To investigate the band composition of the doped system, we further study the projected density of states (PDOS), as shown in Fig. 4. The s states of the non-metal appear near the bottom of the VB with a deeper level, while most p states of the non-metal are involved in the composition of the top of the VB, except a tiny amount of p states appearing in the CB. For N and S doped Bi_2O_3, the 3p state peaks of N and S have broad distributions, ranging from −6 eV to 0.5 eV, as a result, the orbital electrons have a much stronger delocalization. The hybridization between the np states of the non-metal and O 2p also contributes to forming a highly dispersive VB. The impurity level (from −6.03 eV to 1.38 eV) is mainly made up by C 2p for the C doped Bi_2O_3, while Bi 6p states constitute that of the halogen element (F, Cl, and Br) doped α-Bi_2O_3. For F, Cl, and Br doped Bi_2O_3, there are no great changes on the width and the composition of the band except the band as a whole moves towards the low energy level. Comparing the PDOS with the band structures, all the results are in fairly good correspondence, particularly for the VB.

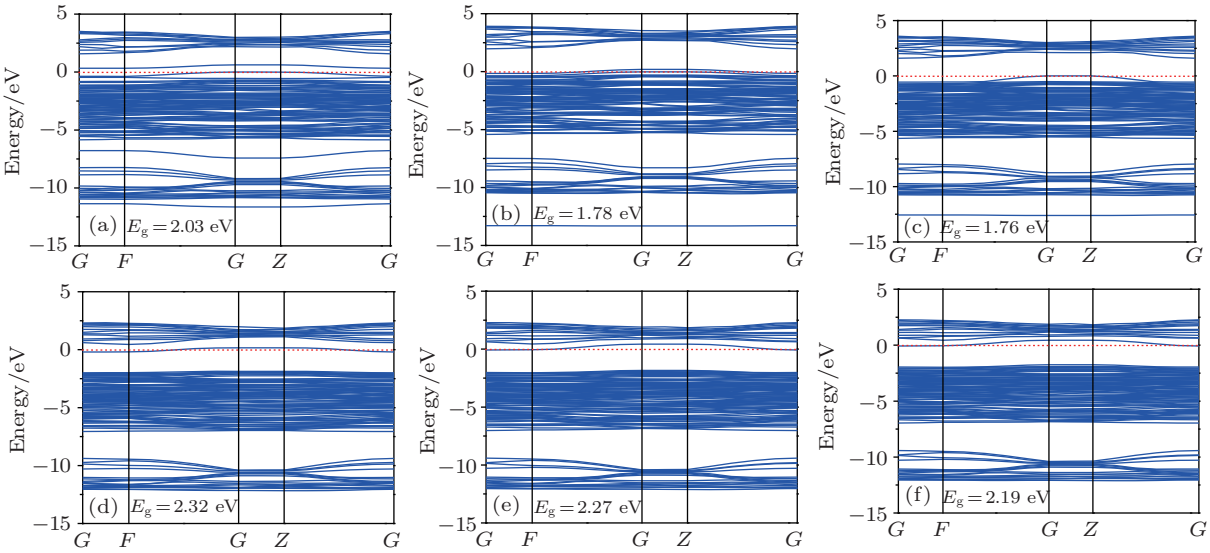


Fig. 3. (color online) Calculated band structure of $Bi_{16}O_{23}M$, where M is respectively C, N, S, F, Cl, and Br in panels (a)–(f).

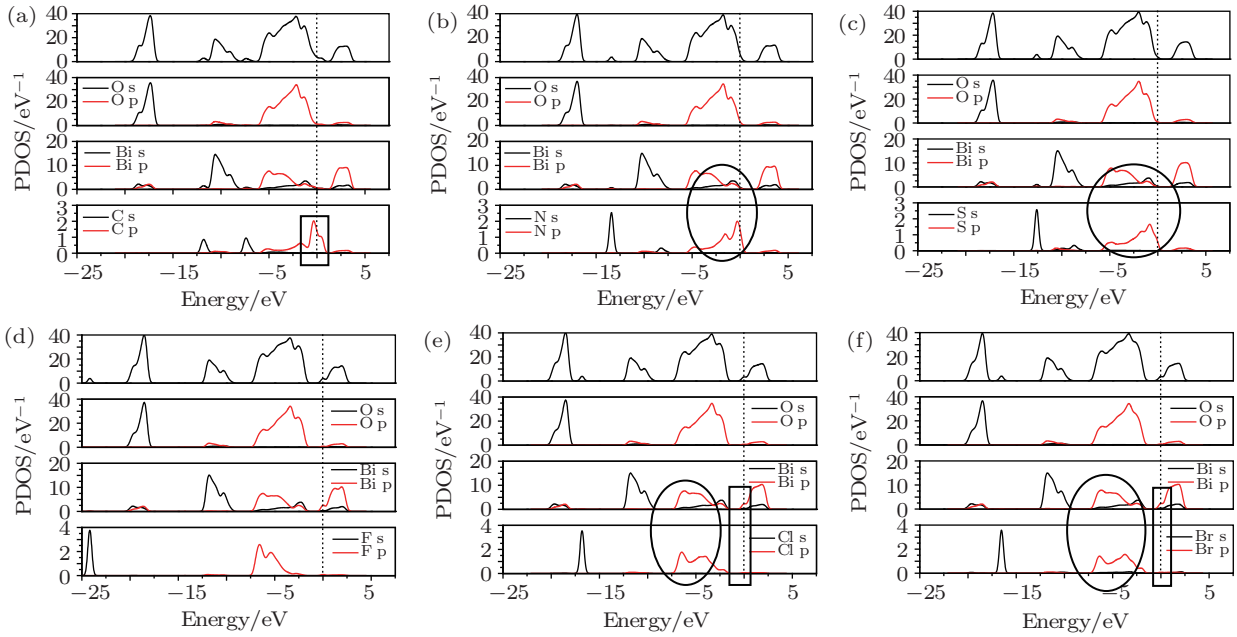


Fig. 4. (color online) Total density of states of $Bi_{16}O_{23}M$ and the corresponding local partial density of states, where M is respectively C, N, S, F, Cl, and Br in panels (a)–(f).

In order to further study the non-metal doping effect, we calculate the effective mass of the electron on the bottom of the CB and that of the hole on the top of the VB, and the results are shown in Table 2. The light effective mass of hole or electron means that the photo-induced charge carrier can be transferred rapidly. The effective mass of the electron for all doped systems is reduced, and the effective mass of the hole is decreased except for F and Cl doped Bi_2O_3, consistent with the results of the PDOS and the band structure. Particularly, the effective masses of electron and hole for N and S doped Bi_2O_3 are greatly reduced, which is accordant with the dispersive band structures. It implies that more carriers can move to the surface of the semiconductor in a typical redox reaction within limited time in the N and S doped Bi_2O_3 samples.

Table 2. The minimum effective mass of the hole on the top of the VB and that of the electron on the bottom of the CB for $Bi_{16}O_{23}M$ (M = C, N, S, F, Cl, Br).

	m_e/m_0	m_h/m_0	E_g
Pure α-Bi_2O_3	0.68	1.43	2.39
C-O	0.51	1.32	2.03
N–O	0.45	1.12	1.78
S–O	0.68	0.71	1.68
F–O	0.43	1.96	2.32
Cl–O	0.39	1.74	2.27
Br–O	0.41	1.39	2.19

The non-metal can affect the electron structure according to the calculations. Particularly, N and S dopings not only narrow the band gap, but also reduce the effective mass of the carriers, which are advantageous for the photocatalytic performance. In order to verify the calculation results, we prepared non-metal N and S doped α-Bi_2O_3 powders, and evaluated their visible-light photocatalytic activities.

3.2. Experimental verification

Figure 5 shows the XRD patterns of N and S doped α-Bi_2O_3. All peaks are assigned to bismite crystallized in the monoclinic form according to JCPDS file No. 41-1449 (space group $P121/C1$, $a = 5.8499$ Å, $b = 8.1698$ Å, $c = 7.5123$ Å, $\beta = 112.988°$). The sharp diffraction lines of the Bi_2O_3 patterns indicate that the powder has a high degree of crystallinity. Meanwhile, the incorporation of N and S does not break the crystal structure of Bi_2O_3. Thus non-metal N and S doped Bi_2O_3 were synthesized.

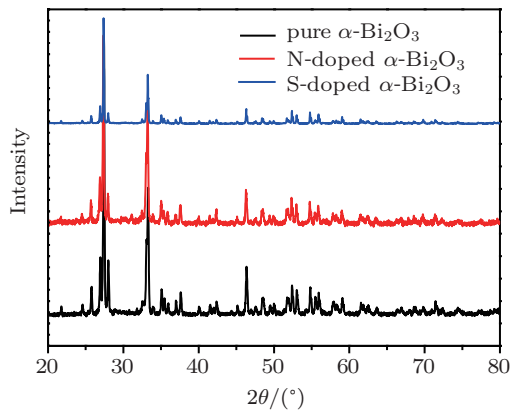


Fig. 5. (color online) X-ray diffraction patterns of pure α-Bi_2O_3 and N/S doped α-Bi_2O_3.

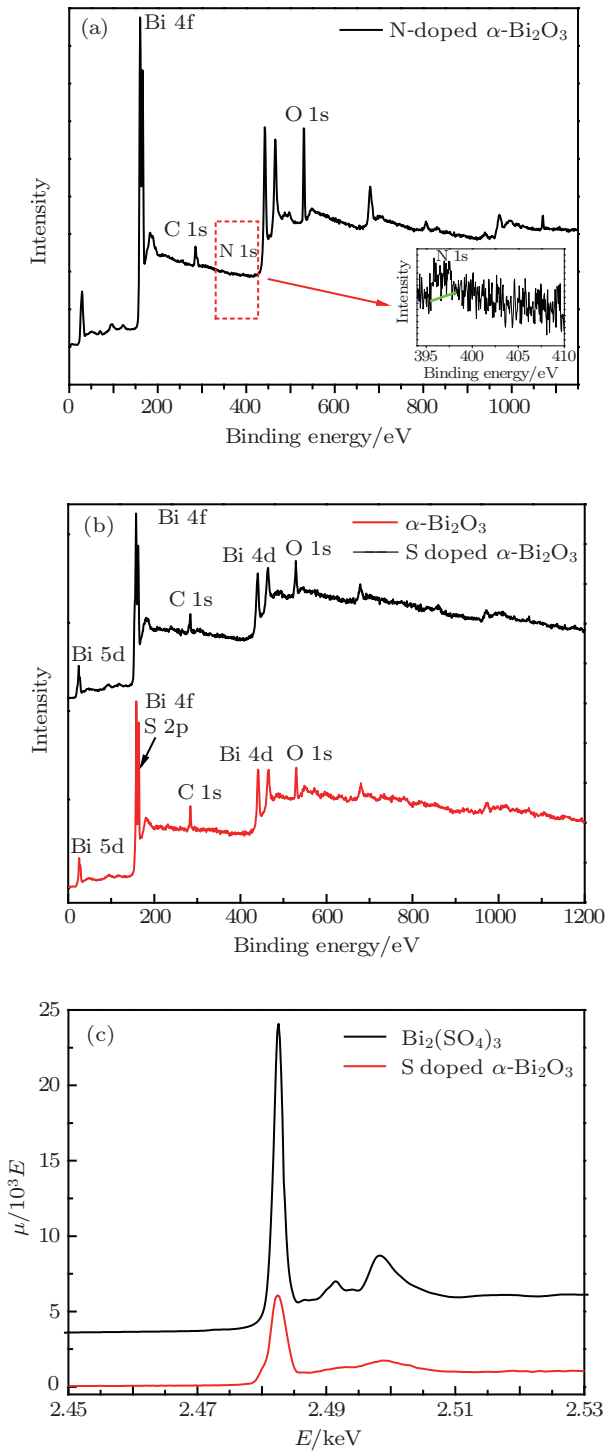


Fig. 6. (color online) (a) XPS of N-doped Bi_2O_3, (b) XPS of S-doped Bi_2O_3, (c) XANES of S in S-doped Bi_2O_3 and $Bi(SO_4)_3$.

In order to check whether N/S is doped into α-Bi_2O_3 or not, XPS of N/S doped α-Bi_2O_3 is detected and shown in Fig. 6. The N 1s peak at 395.5 eV is found in the XPS of N doped α-Bi_2O_3. This result proves the success of N doping into Bi_2O_3. In Fig. 6(b), the S 2p peak at 164.0 eV is found. This confirms the existence of S in the S-doped α-Bi_2O_3 sample. However, the S 2p peak overlaps with the Bi 4f peak, which leads to a difficulty in distinguishing between these two peaks. In order to further prove the existence of the S element, XANES of S element is obtained and shown in Fig. 6(c). The S-doped Bi_2O_3 sample has the same characteristic peak as that of S from $Bi(SO_4)_3$, which demonstrates the success of S doping into Bi_2O_3. Furthermore, the S in S-doped Bi_2O_3 has the same valence state as that in $Bi(SO_4)_3$.

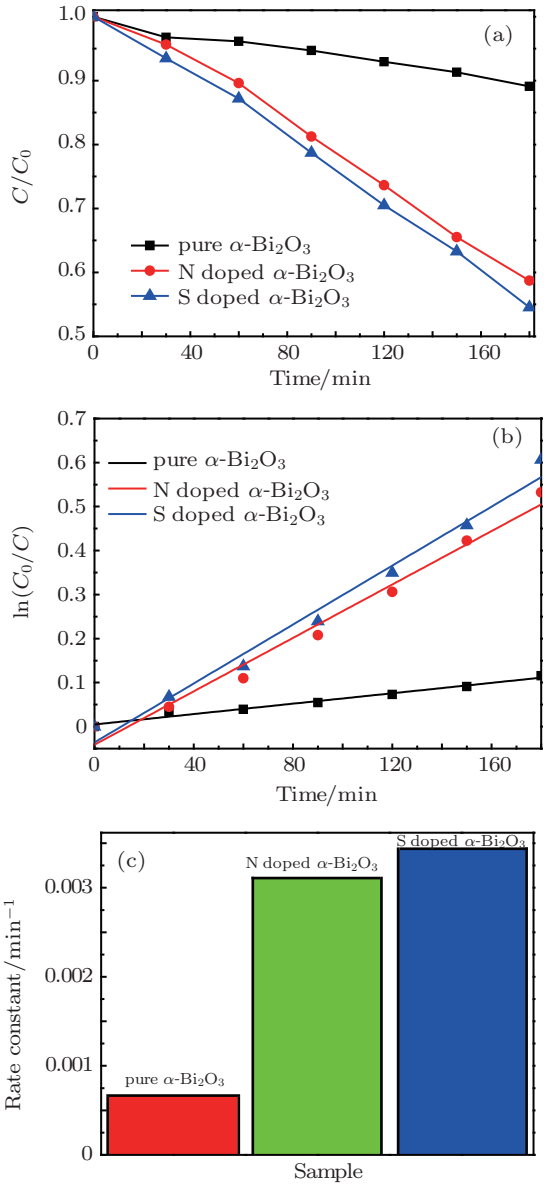


Fig. 7. (color online) Photocatalytic degradation of RhB for pure and N/S doped α-Bi_2O_3: (a) the decolorization of RhB, (b) logarithmic plot of the decolorization, (c) rate constant of the first order reaction.

Figure 7 shows degradation tests of RhB over pure and N/S doped Bi_2O_3. All the α-Bi_2O_3 samples show visible-light photocatalytic activities. The discoloration rates of RhB are 10.9%, 41.28%, and 45.5% for pure Bi_2O_3, N and S doped Bi_2O_3, respectively. Since the Langmuir–Hinshelwood model has been widely used to investigate the photocatalytic process, the apparent rate constant k is chosen as the basic kinetic parameter for different photocatalysts. The first order kinetic equation is used to fit experimental data in Fig. 7(a)

$$\ln(C_0/C) = kt, \tag{1}$$

where C is the concentration of RhB remaining in the solution at irradiation time t, and C_0 is the initial concentration at $t = 0$. The variation in $\ln(C_0/C)$ as a function of the irradiation time is given in Fig. 7(b). The calculated k values are 0.00059 min^{-1}, 0.00303 min^{-1}, and 0.00335 min^{-1} for pure Bi_2O_3, N and S doped Bi_2O_3, respectively. Apparent rate constants are clearly displayed in the histogram, as shown in Fig. 7(c). It confirms that the photocatalytic activity has been indeed enhanced by non-metal doping as expected.

4. Conclusion

In summary, the electronic structures and the photocatalytic properties of pure and non-metal (C, N, S, F, Cl, and Br) doped α-Bi_2O_3 are investigated by first-principles calculations based on the DFT. The N and S doped Bi_2O_3 not only have narrow band gaps but also possess light effective masses of electrons and holes, which are beneficial for photocatalysis. Experimental results for the photocatalytic activity of N and S doped Bi_2O_3 are consistent with the theoretical calculations. The theoretical calculation is a reliable tool to predict the electronic structure of oxides doped with non-metals.

References

[1] Mills A, Davies R H and Worsley D 1993 *Chem. Soc. Rev.* **22** 417
[2] Konstantinou I K and Albanis T A 2004 *Appl. Catal. B Environ.* **49** 1
[3] Deng H Y, Hao W C, Xu H Z and Wang C Z 2012 *J. Phys. Chem. C* **116** 1251
[4] Fujishima A and Honda K 1972 *Nature* **238** 37
[5] Zou Z G, Ye J H, Sayama K and Arakawa H 2001 *Nature* **414** 625
[6] Kudo A and Misek Y 2009 *Chem. Soc. Rev.* **38** 253
[7] Chen X B and Mao S S 2007 *Chem. Rev.* **107** 2891
[8] Li X Z and Li F B 2001 *Environ. Sci. Technol.* **35** 2381
[9] Xu J J, Ao Y H, Fu D J and Yuan C W 2008 *Appl. Surf. Sci.* **255** 2365
[10] Gao P, Wu J, Liu Q J and Zhou W F 2010 *Chin. Phys. B* **19** 087103
[11] Li C Y, Wang J B and Wang Y Q 2012 *Chin. Phys. B* **21** 098102
[12] Sathish M, Viswanathan B, Viswanath R P and Gopinath C S 2005 *Chem. Mater.* **17** 6349
[13] Park J H, Kim S and BardZh A J 2006 *Nano Lett.* **6** 24
[14] In S, Orlov A, Berg R, García F, Pedrosa-Jimenez S, Tikhov M S Wright D S and Lambert R M 2007 *J. Am. Chem. Soc.* **129** 13790
[15] Chen X and Burda C 2008 *J. Am. Chem. Soc.* **130** 5018
[16] Hitoki G, Takata T, Kondo J N, Hara M, Kobayashib H and Domen K 2002 *Chem. Commun.* 1698
[17] Kasahara A, Nukumizu K, Takata T, Kondo J N, Hara M, Kobayashi H and Domen K 2003 *J. Phys. Chem. B* **107** 791
[18] Ishikawa A, Takata T, Kondo J N and Hara M 2002 *J. Am. Chem. Soc.* **124** 13547
[19] Zhou J K, Lv L, Yu J, Li H L, Guo P Z, Sun H and Zhao X S 2008 *J. Phys. Chem. C* **112** 5316
[20] Wei W, Dai Y and Huang B B 2009 *J. Phys. Chem. C* **113** 5658
[21] Vurgaftman I, Meyer J R and Ram-Mohan L R 2001 *J. Appl. Phys.* **89** 5815
[22] Zou W, Hao W C, Xin X and Wang T M 2009 *Chin. J. Inorg. Chem.* **25** 1971
[23] Imanaka N, Masui T, Imadzu H and Yasuda K 2011 *Chem. Commun.* **47** 11032
[24] Wang Y, Wen Y Y, Ding H M and Shan Y K 2010 *J. Mater. Sci.* **45** 1385
[25] Eberl J and Kisch H 2008 *Photochem. Photobiol. Sci.* **7** 1400
[26] Carlsson J M, Hellsing B, Domingos H S and Bristowe P D 2002 *Phys. Rev. B* **65** 205122
[27] Sammes N M, Tompsett G A, Nafe H and Aldinger F 1999 *J. Eur. Ceram. Soc.* **19** 1801
[28] Kumari L, Lin J H and Ma Y R 2007 *J. Phys.: Condens. Matter* **19** 406204